

Theoretical Investigation of Interstellar 3-Pyrroline: Formation, Rotational and Vibrational Spectroscopy

Anshika Pandey,^{*} Akant Vats, Satyam Srivastav, Amit Pathak[†] and K. A. P. Singh

Department of Physics, Institute Of Science, Banaras Hindu University, Varanasi-221005, India

Accepted XXX. Received YYY; in original form ZZZ

ABSTRACT

The recent detection of CN-functionalized aromatics partly addresses the long-standing mystery of the apparent absence of five- and six-membered rings in interstellar environments. N-heterocycles, which are crucial as the fundamental structures of nucleobases, have been a focus of these aromatic searches due to their biological significance. Although N-heterocycles have not been conclusively detected in astrophysical environments, their presence in chondrites and meteorites signifies their interstellar and circumstellar connection. Precise spectral data identifies the unique signatures of molecules, confirming their presence in space. In this light, the present work reports an extensive computational investigation on interstellar 3-pyrroline; a five-membered ring N-heterocycle. This includes an alternative formation route in cold interstellar environments and highly accurate rotational and vibrational spectroscopy. The results indicate that 3-pyrroline can form on dust grain surfaces from vinyl cyanide, as its formation from pyrrole through double hydrogenation may lead to the formation of pyrrole itself via a H₂ abstraction process. 3-pyrroline's rotational transition at 52.3 GHz offers a potential tool for its detection in cold interstellar regions. Additionally, the strongest infrared features of 3-pyrroline at 16.09 μ m and \sim 3.50 μ m are observable with JWST. The provided data is crucial for laboratory identification and future interstellar observations of 3-pyrroline at both radio and IR wavelengths.

Key words: astrochemistry — molecular processes — line: identification — ISM: molecules — radio lines: ISM — infrared: ISM.

1 INTRODUCTION

While different classes and types of organic molecules have been detected in the interstellar medium (ISM) (McGuire 2022), there was no astronomical signature of branched chain molecules (BCMs) and polycyclic aromatic hydrocarbons (PAHs) until the last decade. Thanks to recent strides in both ground- and space-based radio and infrared telescopes, such as ALMA (Wootten & Thompson 2009), GBT (Lockman 1996), and JWST (Gardner et al. 2006), it is now possible to delve into the evolved realms of interstellar physics and chemistry. BCM was first detected in the form of *iso*-propyl cyanide (*i*-C₃H₇CN) (Belloche et al. 2014; Pagani et al. 2017), and recently PAHs have been identified mainly in the form of CN-functionalized aromatics (McGuire et al. 2018, 2021; Cernicharo et al. 2021a; Burkhardt et al. 2021; McCarthy et al. 2021a; Sita et al. 2022). The detection of both the BCM and CN-PAHs is of great importance because they could potentially serve as a building block for life due to the side chain structure, aromaticity, and the presence of carbon and nitrogen atoms—basic chemical ingredients necessary for life. Having successfully identified several aromatic compounds, the exploration of nitrogen (N)-heterocyclic molecules (where an N atom is a member of a ring) emerges as the next natural progression in unraveling the chemical complexity of interstellar environments (e.g. Barnum et al. 2022).

N-heterocycles hold immense biological importance as they serve as the fundamental structure of nucleobases, which are the building blocks of DNA and RNA responsible for carrying the genetic information of living organisms (e.g. Barnum et al. 2022). However, until now, no five- or six-membered ring heterocycles have been unequivocally identified in the ISM. Several N-heterocycles, for e.g., imidazole, pyridine, pyrimidine, pyrrole, indole, quinoline, and isoquinoline have been searched towards different astronomical regions, with unsuccessful detection (Barnum et al. 2022, and references therein). Despite their non-detection, N-heterocycles have been detected in several chondrites (Hayatsu 1964; Folsome et al. 1971, 1973; Hayatsu et al. 1975; van der Velden & Schwartz 1977; Komiya et al. 1993), which strongly signifies their interstellar and circumstellar connection (Barnum et al. 2022). Moreover, observations of PAH IR emission bands strongly support the significant abundance of N-heterocycles in the ISM (Tielens 2008), with the 6.2 μ m PAH emission band in interstellar environments believed to originate from PAH carriers containing nitrogen in their structures. (Hudgins et al. 2005; Ricca et al. 2021; Vats et al. 2022).

Pyrrole (C₄H₅N), a significant interstellar N-heterocycle, has been searched towards the hot core Sgr B2(N) with a column density of 3–6 \times 10¹³ cm^{–2} (Myers et al. 1980), and the cold molecular cloud TMC-1, where the column density is 4 \times 10¹² cm^{–2} (Kutner et al. 1980). Pyrrole can produce several other N-heterocycles in the ISM, such as pyridine (C₅H₅N) with methylidyne radical (CH) (Barnum et al. 2022) and 2- and 3-pyrrolines (C₄H₇N) with its hydrogenation

^{*} E-mail: 3anshika.1@gmail.com

[†] E-mail: amitpah@gmail.com

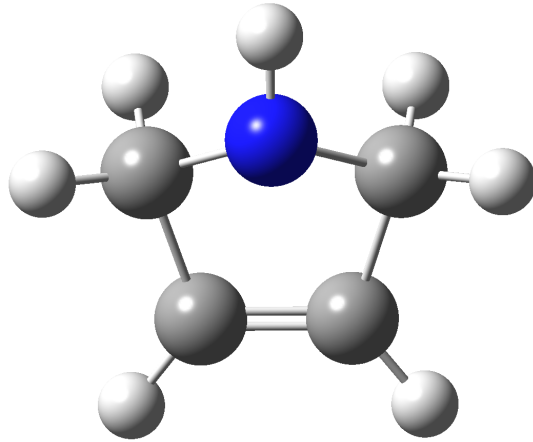


Figure 1. Structural depiction of 3-Pyrroline.

(Mikscha et al. 2021). It is important to note here that both pyrrole and pyrrolines have an NH bond in their structures.

The detection of cyanocyclopentadiene (c-C₅H₅CN), a five-membered ring molecule containing a CN group, raises questions about why pyrrole hasn't been observed even though both are found to have comparable column densities (McCarthy et al. 2021a).

McGuire et al. (2018) and McCarthy et al. (2021a) propose one of the two following arguments to explain this. Firstly, it's conceivable that a significant portion of N might not be present primarily in the NH form, whose reaction with butadiene is considered a significant route leading to the formation of pyrrole. Another potential scenario is that the process of cyanation effectively transforms pre-existing aromatic substances, yielding c-C₅H₅CN and other rings with CN-functionalization. The formation of 3-pyrroline from pyrrole depends on two successive H-addition reactions at pyrrole's carbon-sites adjacent to the N atom where there is a slight possibility of a H₂ abstraction process leading to the formation of pyrrole itself (Mikscha et al. 2021). However, Mikscha et al. (2021) suggests that 2 and 3-pyrroline are promising candidates for future astronomical searches, with 3-pyrroline being the most stable isomer (Boggs & Kim 1985). This further hints at the potential to search for 3-pyrroline in the ISM, which could shed more light on the N-heterocycles' chemistry. Due to our incomplete understanding of pyrrole formation, it remains plausible that 3-pyrroline could be undergoing alternative chemical routes within the ISM besides its association with pyrrole.

In view of the above, the present work explores an in-depth theoretical investigation of 3-pyrroline in interstellar conditions. This involves a reaction mechanism for the formation of 3-pyrroline from vinyl cyanide (CH₂CHCN), one of the most readily detected and fundamental nitriles in the ISM. We also report accurate rotational and vibrational spectroscopy of 3-pyrroline to facilitate its astronomical searches in diverse interstellar regions. The rotational spectra are studied at three different temperatures (5, 10, and 100 K) to encompass the range of conditions found in N-heterocycle searches, including both cold sources like TMC-1 and warmer environments like Sgr B2. Given the success of hyperfine-resolved structures in identifying molecules within cold environments, such as CN-PAHs in TMC-1 (e.g. McGuire et al. 2018, 2021), we present the hyperfine resolved spectrum of 3-pyrroline at 5 K. The highly accurate IR spectrum of 3-pyrroline, which incorporates anharmonic effects, is presented here in light of the JWST ushering in a new era of unparalleled IR sensitivity. This sensitivity opens the door to potentially detecting single molecules. We further investigate how the vibrational spectra

of 3-pyrroline change as the concentration of H₂O ice increases. This is particularly relevant because water ice is a dominant component in dense interstellar clouds. The paper is organized as follows. Section 2 outlines the computational and theoretical methods employed. Section 3 presents the results along with their astrophysical implications, and Section 4 summarizes the conclusions.

2 COMPUTATIONAL DETAILS

All the quantum chemical calculations here have been performed using Density Functional Theory (DFT) with Gaussian 16 (Frisch et al. 2016) suite of programs.

The formation of 3-pyrroline was investigated by employing the B3LYP functional (Lee et al. 1988; Becke 1993) with Dunning's correlation-consistent basis set augmented with diffuse functions, aug-cc-pVTZ (Dunning 1989) and considering dispersion effects-D3(BJ) (Grimme et al. 2011). We first optimize the reactants and products of each step to calculate the transition states (TS) with the QST2 method (Peng & Bernhard Schlegel 1993). The B3LYP/aug-cc-pVTZ, is widely used to study reaction mechanisms in the ISM (Tonolo et al. 2020; Flint & Fortenberry 2022; Redondo et al. 2023; Martínez-Bachs & Rimola 2023). The same methodology has been employed to calculate reaction enthalpies and Gibbs free energies. Additionally, we perform single-point energy calculations for the TS and the optimized reactant structures at the CCSD(T)/aug-cc-pVTZ level to correct the barriers more accurately. Frequency analysis confirmed minima and transition states, with TS geometries connecting minima explored via intrinsic reaction coordinates (IRC). To mimic the characteristics of ice, molecules in the reaction network are embedded in a continuous solvation field to simulate local effects. This is achieved using the default self-consistent reaction field (SCRF) method, specifically the integral equation formalism (IEF) variant of the polarizable continuum model (PCM), with water acting as the solvent (Cancès et al. 1997; Tomasi et al. 2005). Studies have found that an implicit solvation model is preferable to mimic the water ice environments. While explicit water molecules can create a more realistic (inhomogeneous) field, the uncertainty regarding the typical size of interstellar water clusters (i.e., the number of water molecules required) led us to prefer using the SCRF method (Woon 2002; Mondal et al. 2021). The implicit solvation model places the molecule inside a cavity within a uniform dielectric medium, like water, representing the solvent. This method works well for simulating ices. The PCM accounts for the reaction field of bulk ice. The reaction fields issuing from a dielectric constant of 78 for water and about 100 for ice (Aragones et al. 2011) are very similar. Thus, the solid-phase calculations and thermochemical parameters here are similar to those in ice.

Binding energies (BEs) determine the residence time of molecules on grain surfaces and are crucial for astrochemical models to accurately predict molecular abundances in the ISM (He et al. 2016; Wakelam et al. 2017; Gorai et al. 2017; Duflot et al. 2021). Therefore, we have calculated the BEs of reactants, intermediates, and products involved in the reaction using a water cluster of tetramer size as a substrate due to its effectiveness in explaining chemical models (Das et al. 2018a). Here, BEs are computed at the B3LYP-D3(BJ)/aug-cc-pVTZ level of theory to examine the comparative BEs of reactants, intermediates, and products with water ices, using the following equation.

$$\text{BE} = (E_{\text{substrate}} + E_{\text{species}}) - E_{\text{ads}}.$$

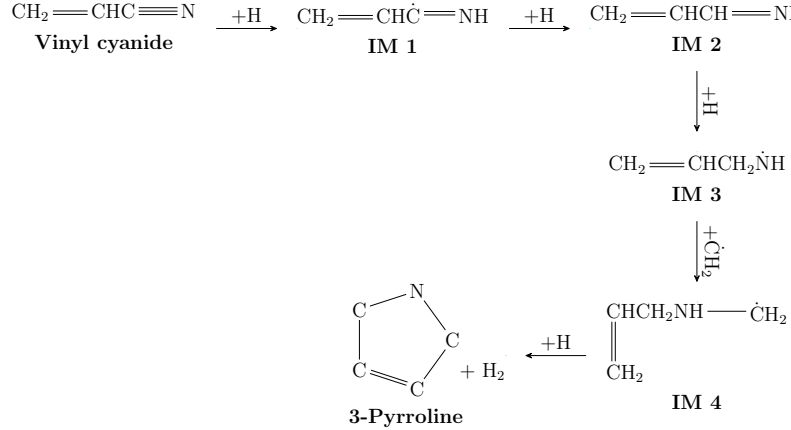


Figure 2. Formation of 3-Pyrroline from vinyl cyanide.

Where, $E_{\text{substrate}}$ and E_{species} are the optimized energies of the grain substrate and species, respectively, where both are obtained separately. E_{ads} is the total calculated energy of the species adsorbed on the surface.

Rotational constants (A, B, C) dictate the intricate spectral fingerprints in rotational spectroscopy. For interstellar environments, rotational constants in the ground vibrational state are crucial. These constants primarily consist of equilibrium rotational values with minor corrections due to vibrational effects (Puzzarini et al. 2023a). The equilibrium constants were calculated using the PCS (Pisa Composite Scheme)/Bonds model (Barone et al. 2023; Barone 2023a,b) beginning with geometries optimized by the revDSD-PBEP86-D3(BJ) functional combined with the 3F12⁻ basis set (Barone & Lazzari 2023). This model incorporates both complete basis set extrapolation and core-valence correlation effects. These inclusions significantly improve the accuracy of calculations for medium- to large-sized molecules, typically by an order of magnitude. The vibrational corrections are acquired by the B3LYP-D3(BJ)/6-31+G* semidiagonal cubic force fields for a good comparison with experimental ground-state rotational constants. The method delivers highly accurate results for N-heterocycles compared to experiments (better than 0.1%) like pyridine (within 0.06% error) and pyrrole (within 0.02% error) (Barone & Lazzari 2023). This accuracy makes PCS/Bonds the ideal choice for studying 3-pyrroline.

Nuclear quadrupole coupling constants and distortion constants were calculated using frozen core approximation coupled cluster method with the perturbative treatment of triple excitations ((fc-CCSD(T)) with the aug-cc-pVTZ basis set in CFOUR (Matthews et al. 2020). This method has been extensively used for the calculation of spectroscopic constants (Puzzarini & Stanton 2023; Puzzarini et al. 2023b). The calculation of nuclear quadrupole coupling constants, χ_{ij} , requires the calculation of the electric field gradient at the quadrupolar nucleus

$$\chi_{ij} = \mathbf{eQ} \times \mathbf{q}_{ij}$$

here, i and j denote the inertial axes, \mathbf{eQ} stands for the nuclear quadrupole moment, and \mathbf{q}_{ij} denotes ij -th element in the electric field gradient tensor (Gordy 1953; Puzzarini et al. 2010).

We have utilized the PGOPHER general purpose software (Western 2017) to simulate the rotational spectra. All spectra have been simulated with rotational-vibrational coupling, anharmonic, quartic centrifugal-distortion, and nuclear quadrupole coupling corrections

at the Vibrational second-order perturbation theory (VPT2) level using Watson's S-reduced asymmetric rotor Hamiltonian I^r axis representation. Pickett's SPCAT (Pickett 1991) program was used to predict transitions for the target molecules, accompanied by estimated errors, and presented them in the JPL standard catalog format. This format facilitates convenient searches for the considered molecule in space.

VPT2 utilizes quadratic, cubic, and quartic force constants to compute anharmonic vibrational frequencies for polyatomic molecules. Additionally, a new generalized version (GVPT2) has been developed to variationally handle near-resonant terms, which is particularly needed for the molecules having CH and NH stretching regions in their IR spectra (Barone 2005; Barone et al. 2010; Bloino & Barone 2012). Within the GVPT2 model, vibrational anharmonicities, mode couplings, and resonances can be efficiently addressed for both energy levels and intensities (e.g. Yang et al. 2021). In this work, the anharmonic IR absorption spectra of 3-pyrroline were computed utilizing GVPT2 using B3LYP-D3(BJ) with N07D basis set (Barone & Cimino 2008) with very tight optimization and a superfine grid. The B3LYP-D3(BJ) method is typically used for examining weakly bonded systems to understand the influence of weak interactions on anharmonic IR spectra. The B3LYP-D3(BJ)/N07D method yields highly accurate results for anharmonic IR spectra of aromatic molecules, with the agreement between theory and experiment within 1% reducing to 0.1% for CH stretching region in PAHs (Mackie et al. 2018). The GVPT2 approach in Gaussian 16 has been proven accurate for addressing anharmonicity in the IR spectra of PAH-related molecules, as demonstrated with pure and nitrogen-containing PAHs (carbon atoms ≥ 22) (Chen 2018; Lemmens et al. 2021). In general, GVPT2 includes a dual-phase process: initially, resonant terms are singled out using an ad hoc test (Martin et al. 1995) and subsequently eliminated, which is termed as deperturbed VPT2 (DVPT2). In the second phase, the eliminated terms are reintroduced via a variational approach. This method is acknowledged for yielding highly precise outcomes (Martin et al. 1995; Barone et al. 2014; Mackie et al. 2015, 2016; Chen 2018; Lemmens et al. 2021; Yang et al. 2021; Franke et al. 2021; Esposito et al. 2024). For example, the majority of the anharmonic wavenumbers computed with GVPT2 for pyrrole ($\text{C}_4\text{H}_5\text{N}$), a molecule similar to 3-pyrroline ($\text{C}_4\text{H}_7\text{N}$), align with experiment within 5 cm^{-1} (Barone et al. 2014).

As H_2O molecules constitute a substantial fraction of interstellar ice mantles within dense interstellar environments, we have also focused on examining the infrared features of 3-pyrroline in the pres-

ence of increasing concentrations of H_2O . Specifically, we investigated how varying concentrations of water impact the fundamental absorption bands of 3-pyrroline. To explore these effects, we computed the IR spectra of 3-pyrroline in the presence of increasing numbers of H_2O monomers, modeling the interaction with water clusters. The structures of the 3-pyrroline water ices investigated here were thoroughly optimized, achieving the three-dimensional arrangement of atoms that minimizes the total energy. Harmonic frequencies were then computed using DFT in conjunction with the B3LYP/aug-cc-pVTZ level of theory. Compared to lower-level basis sets, the aug-cc-pVTZ basis set offers improved accuracy in describing electron-correlation effects, leading to better agreement with experimental data (e.g. [Lignell et al. 2021](#)). The concentrations of H_2O and 3-pyrroline ($\text{C}_4\text{H}_7\text{N}:\text{H}_2\text{O}$) are selected as 1:1, 1:2, 1:3, 1:4, 1:8, 1:10, and 1:16, respectively. These concentrations are chosen to investigate the systematic effect of increasing H_2O concentrations on fundamental IR bands of 3-pyrroline.

3 RESULT AND DISCUSSION

3.1 Probable formation of 3-pyrroline

In the ISM, smaller aromatic molecules with one or two rings, including N-heterocycles, might form locally from simpler building blocks (bottom-up) (e.g. [Doddipatla et al. 2021](#); [Mikscha et al. 2021](#); [McCarthy & McGuire 2021](#); [Barnum et al. 2022](#)). This is supported by the recent discoveries of CN-PAHs and a pure PAH (indene) in dense molecular clouds like TMC-1 ([McGuire et al. 2018, 2021](#); [Burkhardt et al. 2021](#); [Agúndez et al. 2023](#)). Additionally, smaller aromatic molecules (less than 20-30 carbon atoms) likely cannot survive the harsh journey from the diffuse ISM to cold molecular clouds due to destruction by ultraviolet radiation ([Chabot et al. 2020](#)). Therefore, the current section explores the possibility of the formation of 3-pyrroline from vinyl cyanide, which is one of the most abundant and readily identified cyanide in cold, dense molecular clouds as it was detected in various diverse environments of the ISM (e.g. [Gardner & Winnewisser 1975](#); [Schilke et al. 1997](#); [Capone et al. 1981](#); [Matthews & Sears 1983](#); [Agúndez et al. 2008](#)). The high abundance of hydrogen atoms in dense molecular clouds makes H-addition and H_2 -abstraction reactions especially significant, likely playing a key role in the formation of 3-pyrroline from vinyl cyanide. Following this, a series of five steps of chemical reactions for the formation of 3-pyrroline is shown graphically in Figure 2, and the energetics of the reactions are listed in Table 1 with activation barriers, reaction enthalpies, and Gibbs free energies (all ZPE corrected). The intermediate products formed in each step here are depicted as IM 1–IM 4 in Figure 2. The potential energy diagram of these reactions is shown in Figure 3 (a) and Figure 3 (b). The enthalpies (ΔH) and Gibbs free energies (ΔG) possess negative values (Table 1), which shows the exothermic and spontaneous nature of all the reactions.

While H-addition to the carbon atom of the double bond is more viable in vinyl cyanide, the recent detection of protonated vinyl cyanide ([Martinez et al. 2013](#)) suggests that H-addition at the nitrogen site might also occur under specific conditions, particularly on dust grain surfaces in cold ISM regions. This forms the radical $\text{CH}_2\text{CHCH}_2\text{NH}$ (IM 1) with an achievable barrier of 5.68 kcal/mol. This newly formed radical can then react with an H atom without any further barrier, leading to a closed-shell molecule $\text{CH}_2\text{CHCH}_2\text{NH}$ (allylimine; IM 2). Allylimine has been tentatively detected in the G+0.693-0.027 molecular cloud ([Albertson et al. 2023](#)), and in interstellar conditions, imines are also considered as reactive species on dust grain surface

(e.g. [Puzzarini et al. 2023a](#)). Further hydrogenation of allylimine at C (adjacent to N) would lead to a radical intermediate $\text{CH}_2\text{CHCH}_2\text{NH}$ (IM 3) with a barrier of 5.15 kcal/mol. The fourth intermediate product, $\text{CH}_2\text{CHCH}_2\text{NHCH}_2$ (IM 4), is formed through radical-radical reaction when CH_2 present in the dense molecular clouds ([Hollis et al. 1995](#); [Polehampton et al. 2005](#)) reacts at the radical N site. The final step might involve the abstraction of an H atom followed by ring closure, ultimately leading to the formation of 3-pyrroline. However, this final stage remains enigmatic, necessitating additional investigations. It is worth noting that the double hydrogenation of pyrrole to form 3-pyrroline also presents uncertainties. Nevertheless, the existing energetic considerations here suggest a plausible route from vinyl cyanide. The challenge lies in the absence of identified H abstraction partners, prompting the exploration of alternative interstellar reactants like OH to unravel this intriguing pathway further.

The BEs of the reactants, intermediates, and products have been computed and presented in Table 2. This allows for a comparison of the residing time of the molecules and their credibility in the formation reaction on dust grain surfaces as the diffusion of a particle on the grain surfaces is a fraction of its BE ([Cuppen et al. 2017](#)). Since water (H_2O) makes up the predominant portion (~70% by mass) of a grain mantle (e.g. [Das et al. 2010](#); [van Dishoeck et al. 2021](#); [Das et al. 2021](#)), we have calculated the BEs using water tetramers as a substrate due to their efficiency in explaining certain chemical models ([Das et al. 2018a](#)). The calculated BEs should exhibit a variety of values depending upon the various binding sites, so the average of BE values have been taken and provided in Table 2 ([Sil et al. 2017](#); [Das et al. 2018b](#); [Ferrero et al. 2020](#)). Ground state spin multiplicity of the molecules is also noted (Table 2). As shown in Table 2, there is a decrease in the values (from IM 2 to IM 4: 834 K, 722 K, and 573 K, respectively), suggesting easier diffusion of intermediates on the surface, thus promoting the reaction's feasibility. Notably, 3-Pyrroline has the highest binding energy (6884 K), highlighting its potential residence on the grain surface.

3.2 Rotational spectroscopy

Table 3 presents the spectroscopic constants of 3-pyrroline including ground state rotational constants (A_0 , B_0 , C_0), centrifugal distortion constants (D_J , D_{JK} , D_K , d_1 , d_2), quadrupole coupling constants (χ_{aa} , χ_{bb} , χ_{cc}), and dipole moment (μ). 3-Pyrroline is a near oblate type asymmetric top molecule with $\kappa = 0.96$, similar to pyrrole ($\kappa = 0.94$). Compared to molecules of similar size, the rotational constants of 3-pyrroline are relatively higher. For instance, 1- and 2-cyano-cyclopentadiene, a five-membered ring molecule detected in the TMC-1 ([McCarthy et al. 2021b](#)), have a similar number of atoms as 3-pyrroline (12 atoms) show rotational constants as $A_0 \sim 8235$ –8350 MHz, $B_0 \sim 1900$ MHz, $C_0 \sim 1550$ MHz, which are lower than those of 3-pyrroline (Table 3). This makes 3-pyrroline suitable for searching in the ISM in terms of their partition function values expressed as $Q_{\text{rot}} = [(kT/h)^3 (\pi/ABC)]^{1/2}$, which relies on temperature (T) and rotational constants (A, B, and C). The partition function along with dipole moments, is a crucial quantity for a molecule to be detected by radio telescopes. The rotational partition function values (Q_{rot}) of 3-pyrroline for seven CDMS (The Cologne Database for Molecular Spectroscopy) standard temperatures as implemented in the JPL database ([Pickett et al. 1998](#)) along with an additional temperature at 5 K are given in Table 4. The centrifugal distortion and quadrupole coupling constants for 3-pyrroline, given in Table 3, are computed at the fc-CCSD(T)/aug-cc-pVTZ level of theory, which has been reported to perform significantly better compared to ex-

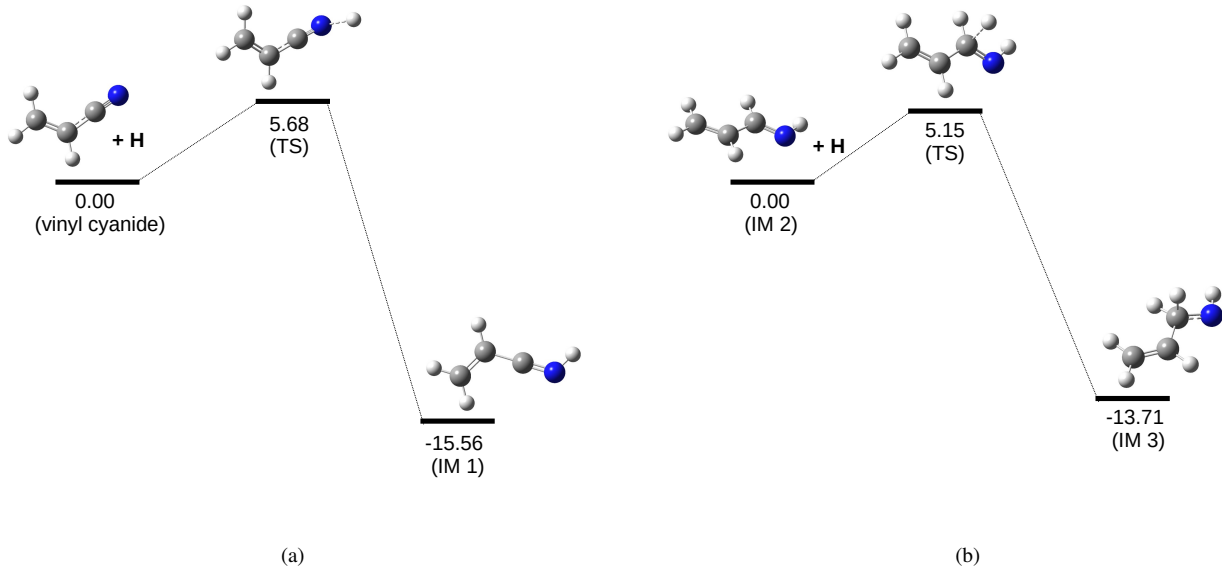


Figure 3. Potential energy diagram for (a) reaction 1, and (b) reaction 3; calculated using CCSD(T)/aug-ccpVTZ level of theory reported in kcal/mol.

Table 1. The ZPE corrected activation barrier at the CCSD(T)/aug-ccpVTZ level of theory, reaction enthalpy and gibbs free energies at the B3LYP/aug-ccpVTZ level of theory.

Reaction number (type)	Reaction Path	Calculated Activation barrier (kcal/mol)	Enthalpy (kcal/mol)	Gibbs Free Energy (kcal/mol)
1 (NR)	$\text{CH}_2\text{CHCN} + \text{H} \rightarrow \text{CH}_2\text{CH}\dot{\text{C}}\text{NH}$	5.68	-21.39	-14.38
2 (RR)	$\text{CH}_2\text{CH}\dot{\text{C}}\text{NH} + \text{H} \rightarrow \text{CH}_2\text{CHCHNH}$	-	-95.59	-86.75
3 (NR)	$\text{CH}_2\text{CHCHNH} + \text{H} \rightarrow \text{CH}_2\text{CHCH}_2\dot{\text{N}}\text{H}$	5.15	-25.28	-18.47
4 (RR)	$\text{CH}_2\text{CHCH}_2\dot{\text{N}}\text{H} + \dot{\text{C}}\text{H}_2 \rightarrow \text{CH}_2\text{CHCH}_2\text{NH}\dot{\text{C}}\text{H}_2$	-	-105.56	-94.17
5 (NR)	$\text{CH}_2\text{CHCH}_2\text{NH}\dot{\text{C}}\text{H}_2 + \text{H} \rightarrow \dot{\text{C}}\text{HCHCH}_2\text{NHCH}_2 + \text{H}_2$	—	—	—

Notes: NR and RR refer to neutral-radical and barrierless radical-radical reactions, respectively.

Table 2. Calculated binding energies of reactant, intermediates, and product with water tetramer at the B3LYP/aug-ccpVTZ level of theory.

Serial number	Species	Ground state	Binding energy H_2O Tetramer (K)
1 (Vinyl cyanide)	CH_2CHCN	Singlet	1294
2 (IM 1)	$\text{CH}_2\text{CH}\dot{\text{C}}\text{NH}$	Doublet	3337
3 (IM 2)	CH_2CHCHNH	Singlet	834
4 (IM 3)	$\text{CH}_2\text{CHCH}_2\dot{\text{N}}\text{H}$	Doublet	722
5 (IM 4)	$\text{CH}_2\text{CHCH}_2\text{NH}\dot{\text{C}}\text{H}_2$	Doublet	573
6 (3-Pyrroline)	$\text{CHCHCH}_2\text{NHCH}_2$	Singlet	6884

periments (within \sim 4-5%) for organic molecules (e.g. Alessandrini et al. 2021; Puzzarini et al. 2024). For dipole moments, 3-pyrroline shows a viable polarity with $\mu_{\text{tot}}=1.5$ D but lower compared to CN-PAHs, which is a common behavior among N-heterocycles with an N atom inside the structure and molecules containing a CN side group (Kisiel et al. 2003; McNaughton et al. 2018; Vávra et al. 2019; Vats & Pathak 2022; Vats et al. 2023). By symmetry, 3-pyrroline has both a-and b-type rotational transitions, with the b-type transition much weaker than the a-type (with $\mu_a = -1.1844$ & $\mu_b = -0.3662$).

Using the accurate rotational, centrifugal distortion, and nuclear quadrupole coupling constants from Table 3, the simulated rotational spectrum of 3-pyrroline is shown in Figure 4. The rotational spectra in Figure 4 are provided at 5 K (red), 10 K (green), and 100 K (blue) temperatures to account for colder and warmer temperature regions

in the ISM. It should be noted that N-heterocycles have been primarily searched in colder regions (McGuire et al. 2018; McCarthy & McGuire 2021; Barnum et al. 2022). The intensity at 100 K is multiplied by a factor of 5, respectively, to account for the influence of a larger partition function that reduces the strength of the transitions with increasing temperature. The most intense rotational transitions of 3-pyrroline at some warmer temperatures fall in the millimeter (110–300 GHz) band, specifically near 200 GHz (215363.8940 MHz). On the other hand, at colder temperatures (at 10 K and 5 K), the transitions having maximum peak intensities lie within the V (40–75 GHz) band, at around 68 GHz (68590.1327 MHz) for 10 K and at around 60 GHz (60470.0734 MHz) for 5 K. Due to the importance of hyperfine resolved spectra in the detection of molecules in colder ISM regions, such as recently detected CN-PAHs in the

Table 3. Spectroscopic parameters (MHz) in the ground state of 3-pyrroline.

3-Pyrroline	
Parameters	B3LYP aug-cc-pVTZ
A_0^a	7698.6674
B_0	7630.0130
C_0	4062.8761
$D_J^b \times 10^6$	893.0330
$D_{JK} \times 10^3$	1.3258
$D_K \times 10^3$	0.2678
$d_1 \times 10^6$	-427.7390
$d_2 \times 10^6$	-140.9430
χ_{aa}^c	3.664
χ_{bb}	1.630
χ_{cc}	-5.295
$(\chi_{bb} - \chi_{cc})$	6.925
μ^d (Debye)	$\mu_a = -1.1844$ $\mu_b = -0.3662$ $\mu_c = 0.0000$ $\mu_{tot.} = 1.5506$

Notes. ^aGround state Rotational constants at revDSD-PBEP86-D3(BJ)/3F12⁻ combined with B3LYP-D3(BJ)/6-31+G* for vibrational corrections, ^bQuartic centrifugal distortion constants, ^c¹⁴N quadrupole coupling constants about the principal inertial axis system, ^dDipole moment calculated at fc-CCSD(T)/aug-cc-pVTZ.

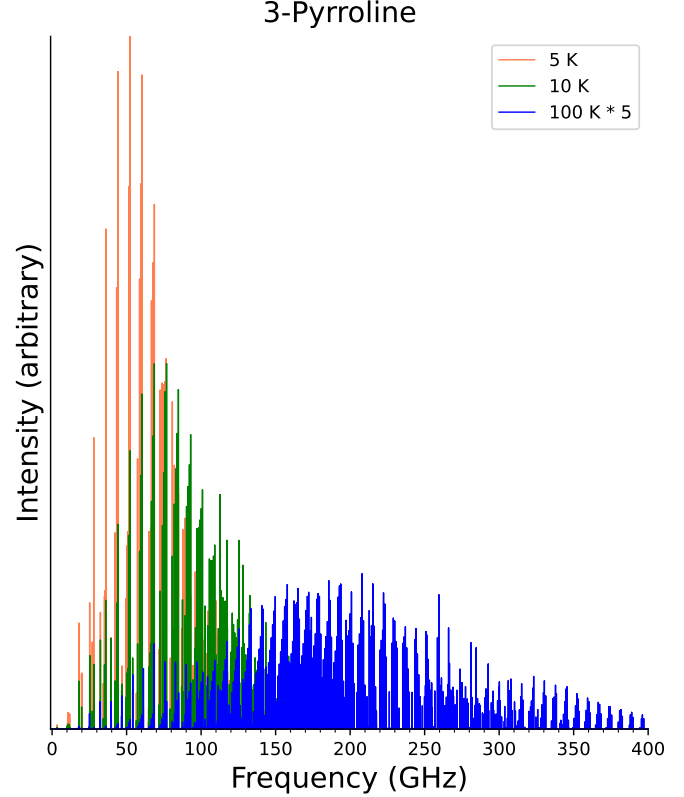
Table 4. Rotational partition function values (Q_{rot}) of 3-pyrroline at given temperatures.

Temperatures (K)	Q^*_{rot}
300.000	28368.4076
225.000	26058.7461
150.000	22113.3889
75.000	14120.5241
37.500	6866.4491
18.750	2650.6082
9.375	946.3981
5.000	370.8478

* $Q_{\text{rot}} = [(kT/h)^3(\pi/ABC)]^{1/2}$, mainly depends on temperature (T) and rotational constants (A,B,C).

TMC-1(for e.g. McGuire et al. 2018), the hyperfine spectra for the strongest transition of 3-pyrroline have been calculated at 10 K, and shown in Figure 5 and transition frequencies are given in Table 5. For 3-pyrroline: the strongest transition at 10 K lies at $J'=6$ around 52.3 GHz in the V band (40–75 GHz) (Figure 5 and Table 5).

Based on the above, the current rotational spectroscopic analysis suggests that 3-pyrroline is a promising candidate for detection in the ISM, specifically in colder regions. The accurate rotational data and lines provided here are intended to guide future laboratory and observational studies. This work concludes that 3-pyrroline could be searched around 52 GHz in colder ISM regions. Further high-resolution experiments are needed to support its radio astronomical detection.

**Figure 4.** Theoretical rotational spectra of 3-pyrroline at 5 K (red), 10 K (green), and 100 K (blue). For display, the relative intensities for the 100 K plot have been multiplied by a factor of 5.**Table 5.** Hyperfine resolved strongest transitions of 3-pyrroline at 5 K.

$J'_{K'_a K'_c} \rightarrow J_{K_a K_c}$	$F'' \rightarrow F'$	5 K
		Calculated Frequency (MHz)
$6_{1,6} \rightarrow 5_{1,5}$	7 → 6	52348.4528
	5 → 4	52348.5212
	6 → 5	52348.6155

3.3 IR spectra of 3-pyrroline

There are several IR lines that indicate the presence of PAHs and PAH derivatives in dense molecular clouds (Bouwman et al. 2011). N-heterocycles, such as 3-pyrroline, are likely to freeze significantly on the ice mantles of dust grains in cold and dense ISM, and their presence can be detected through IR absorption features. For example, a weak band around 3.25 μm due to CH stretch vibrations (e.g. Sellgren et al. 1995), a widely observed feature at 3.47 μm attributed to CH stretching in CH_2 groups (e.g. Chiar et al. 2021), CC stretching and CH out-of-plane bending vibrations at 6.2 μm (Keane et al. 2001), and 11.2 μm (Bregman et al. 2000), respectively, may also contribute to IR absorption features in dense ISM. Since aromatics have been detected in the gas-phase, the accurate IR absorption spectra of 3-pyrroline in gas-phase are depicted in Figure 6, convolved with an FWHM of 1 cm^{-1} and Lorentzian profile for detailed analysis of spectral lines. Due to strong resonances effects in the C-H and N-H stretching regions (~ 2500 – 4000 cm^{-1}), the spectrum is plotted in two ranges: ~ 500 – 2000 , and 2000 – 4000 cm^{-1} with relative intensities (Figure 6). Considering that a significant portion of interstellar

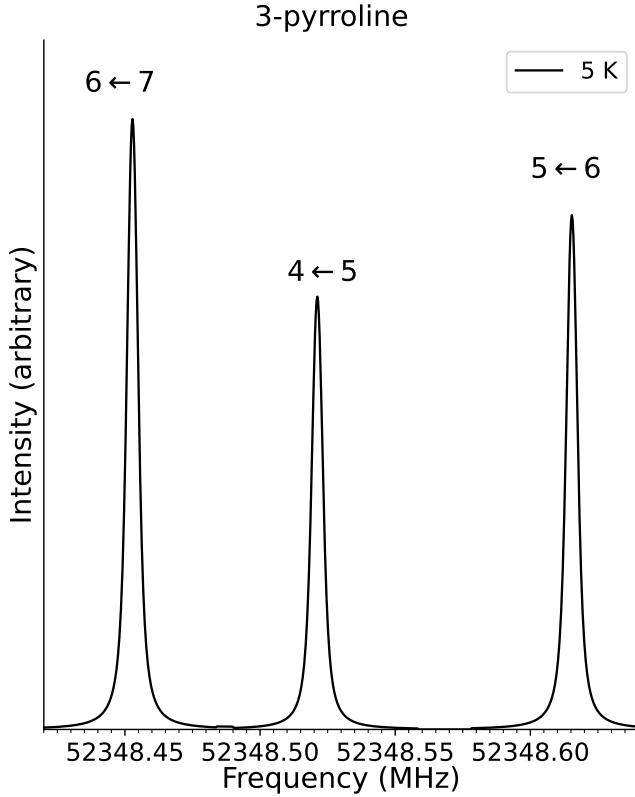


Figure 5. The strongest transition of 3-pyrroline at 5 K ($J'_{K'_a,K'_c} \rightarrow J''_{K''_a,K''_c} = 6_{1,6} \rightarrow 5_{1,5}$) showing the resolved hyperfine structure ($F'' \rightarrow F'$) in the spectrum.

Table 6. Anharmonic IR frequency (cm^{-1} and μm), intrinsic intensity (km mol^{-1}), relative intensity ($I_{\text{rel.}}$), and mode number of 3-pyrroline.

Frequency (cm^{-1})	Intensity (km mol^{-1})	$I_{\text{rel.}}$	Mode
621.38	16.09	79.42	ν_{28}
703.09	14.22	28.42	ν_{27}
770.55	12.97	05.10	$\nu_{30} + \nu_{28}$
785.43	12.73	17.56	$\nu_{30} + \nu_{27}$
799.86	12.50	22.26	ν_{25}
904.25	11.05	03.81	ν_{24}
1037.17	9.64	23.16	ν_{19}
1094.56	9.13	27.27	ν_{18}
1184.92	8.43	04.50	ν_{15}
1414.85	7.06	13.82	ν_{11}
1494.50	6.68	03.10	$\nu_{27} + \nu_{22}$
2633.27	3.79	05.79	$\nu_{14} + \nu_{12}$
2765.11	3.61	09.92	$\nu_{12} + \nu_{11}$
2808.72	3.56	23.81	ν_6
2821.56	3.54	24.39	$2\nu_{11}$
2827.16	3.53	61.59	ν_7
2846.35	3.51	75.84	ν_4
2859.15	3.49	22.46	ν_5
2993.93	3.34	07.63	$\nu_{10} + \nu_9$
3090.27	3.23	14.93	ν_2
3096.58	3.22	04.13	ν_3
3170.06	3.15	23.27	$\nu_{30} + \nu_1$
3700.83	2.70	22.13	$\nu_{28} + \nu_1$

Only modes exceeding 0.04 relative intensity are reported.

dust exists in the form of water (H_2O) ices, IR spectra of 3-pyrroline in the presence of water ices are studied and illustrated in Figure 7, convolved with an FWHM of 8 cm^{-1} and Gaussian profile for a continuous spectra. The anharmonic IR frequencies of gas-phase 3-pyrroline are listed in Table 6, along with intensities at both absolute and relative scales.

In Table 6, the most intense IR features of 3-pyrroline are the ν_{28} and ν_4 fundamentals present at 621.38 cm^{-1} ($16.09 \mu\text{m}$) and 2846.35 cm^{-1} ($3.51 \mu\text{m}$), respectively. The dominant vibrations are NH out-of-plane bending at $16.09 \mu\text{m}$ and CH stretching in CH_2 groups at $\sim 3.50 \mu\text{m}$. Furthermore, the ν_{28} fundamental at $16.09 \mu\text{m}$ lies in a part of the long-wavelength IR spectrum that is relatively free of features from large PAHs (Peeters et al. 2004) and silicates (Molster et al. 2001), making 3-pyrroline a feasible target to search for with JWST or other IR facilities. The observed $3.47 \mu\text{m}$ absorption feature is primarily attributed to ammonia hydrates (Dartois & d'Hendecourt 2001; Dartois et al. 2002), though other sources have been proposed, such as CH stretching in CH_2 groups in PAHs (Chiar et al. 2021). 3-Pyrroline with a strong band (with $I_{\text{rel.}}=0.95$) due to CH stretching in the CH_2 groups can contribute to the observed $3.47 \mu\text{m}$ absorption. Even if ammonia hydrates are the predominant carriers, contributions from hydrogenated PAHs or related species cannot be excluded (Maté et al. 2023). A weak feature (ν_{28} fundamental) due to CH stretching vibrations at $\sim 3.23 \mu\text{m}$ in 3-pyrroline might contribute to the observed $3.25 \mu\text{m}$ absorption. The other strong features are for ν_{27} at 703.09 cm^{-1} ($14.22 \mu\text{m}$, $I_{\text{rel.}}=0.36$), ν_{13} , and at 1094.56 cm^{-1} ($9.13 \mu\text{m}$, $I_{\text{rel.}}=0.34$).

In the presence of water (H_2O) ices, the fundamental vibrational bands of 3-pyrroline show significant changes (Figure 7), indicating a strong interaction between the water molecules and 3-pyrroline. These interactions, likely involving hydrogen bonding and other intermolecular forces, can alter the vibrational modes of 3-pyrroline, leading to shifts in band positions and changes in band intensities. In particular, the strong OH stretching vibrations overshadow the most prominent CH stretching features of 3-pyrroline with increasing H_2O concentrations between $3000\text{--}3500 \text{ cm}^{-1}$. Furthermore, a strong fundamental band in pure 3-pyrroline at $\sim 600 \text{ cm}^{-1}$ ($\sim 16.6 \mu\text{m}$), corresponding to NH out-of-plane bending, with other CH out-of-plane bending features between $\sim 1000\text{--}666 \text{ cm}^{-1}$ ($\sim 10\text{--}15 \mu\text{m}$) fade away in the presence of water dimers and above, compared to the CH stretch region. The increasing concentration of H_2O highly affects the IR bands of 3-pyrroline (Figure 7), presenting challenges in drawing any definitive conclusions for discerning 3-pyrroline features in water ices. This amplifies the likelihood of more possibility of detecting it in the gas phase.

4 CONCLUSIONS

The recent GBT Observations of TMC1: Hunting for Aromatic Molecules (GOTHAM) survey (e.g. McCarthy et al. 2021b; McGuire et al. 2021) and Q-band Ultrasensitive Inspection Journey to the Obscure TMC-1 Environment (QUIJOTE) line survey (e.g. Cernicharo et al. 2021b) suggest that an N-heterocycle similar to 3-pyrroline might exist in the ISM; however, extensive work is needed to confirm this. The present work examines a probable formation route for 3-pyrroline in cold ISM. This work provides highly accurate rotational transitions and IR frequencies to guide laboratory and observational studies. Pyrrolines are generally considered double-hydrogenated forms of pyrrole. However, addition of two hydrogen atoms might not be a stable endpoint. The subsequent loss of a hydrogen molecule (H_2) through abstraction could potentially lead back to

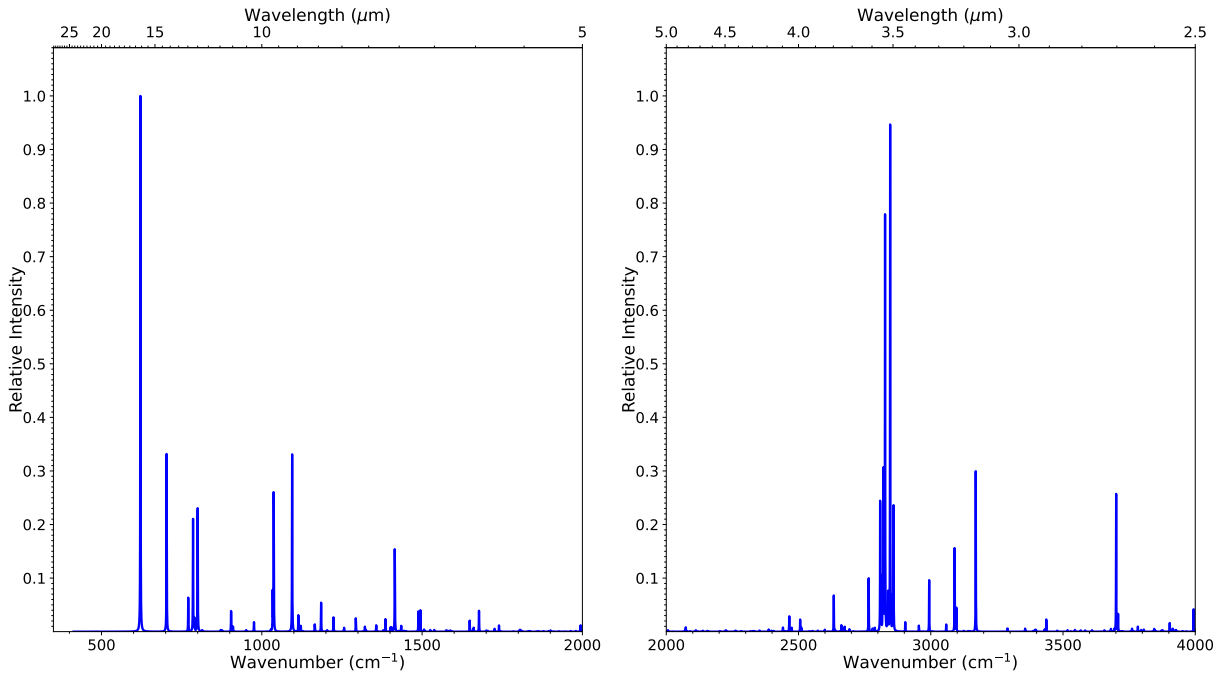


Figure 6. Anharmonic gas phase IR absorption spectra of 3-pyrroline with an FWHM of 1 cm^{-1} and a Lorentzian line profile.

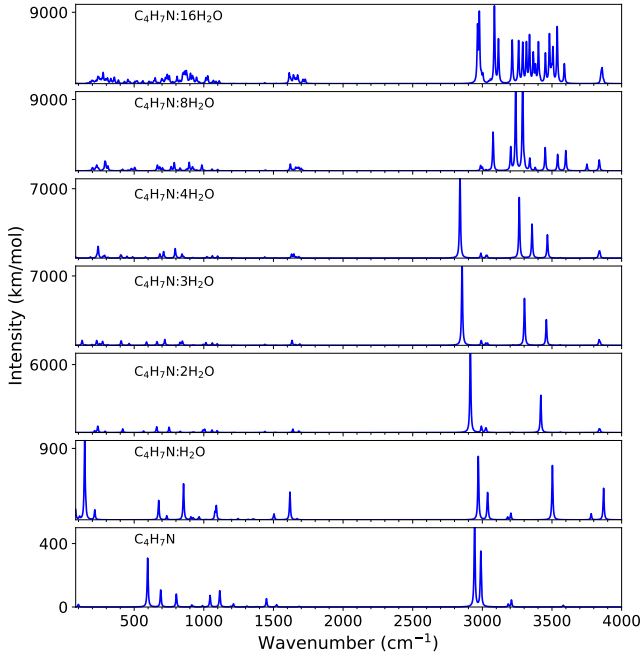


Figure 7. Gas phase harmonic IR absorption spectra of 3-pyrroline with different H_2O concentrations using an FWHM of 8 cm^{-1} and a Gaussian line profile.

the formation of pyrrole itself (Mikscha et al. 2021). The alternative pathway studied here suggests that 3-pyrroline can form on interstellar dust grains with successive hydrogenation of vinyl cyanide, which is the most frequently detected nitrile in space. 3-pyrroline could be searched in cold interstellar environments through its rotational transitions around 52.3 GHz. The most intense IR features of 3-pyrroline are present at $16.09\text{ }\mu\text{m}$, and $\sim 3.5\text{ }\mu\text{m}$, respectively. These funda-

mental features, located in an IR region free from PAH interference, are detectable with JWST. Therefore, the spectral information for the 3-pyrroline presented in this work will be crucial for both its experimental identification and future interstellar observations. Although the current work lays a strong foundation, the complexities of interstellar chemistry necessitate further investigation.

ACKNOWLEDGEMENTS

AP (Anshika Pandey) acknowledges Banaras Hindu University and UGC, New Delhi, India, for providing a fellowship. AV acknowledges research fellowship from DST SERB (SERB-EMR/2016/005266) and UGC. SS acknowledges RJP-PDF, Banaras Hindu University. AP (Amit Pathak) acknowledges financial support from the IoE grant of Banaras Hindu University (R/Dev/D/IoE/Incentive/2021-22/32439), financial support through the Core Research Grant of SERB, New Delhi (CRG/2021/000907) and thanks the Inter-University Centre for Astronomy and Astrophysics, Pune for associateship. KAPS acknowledges the UGC Faculty Recharge Program of Ministry of Human Resource Development (MHRD), Govt. of India and University Grants Commission (UGC), New Delhi, and support from IoE grant of Banaras Hindu University.

DATA AVAILABILITY

On receiving a reasonable request from the corresponding author, the data utilized in this article will be provided.

REFERENCES

Agúndez M., Cernicharo J., Pardo J. R., Fonfría Expósito J. P., Guélin M., Tenenbaum E. D., Ziurys L. M., Apponi A. J., 2008, *Ap&SS*, **313**, 229
Agúndez M., Marcelino N., Tercero B., Cernicharo J., 2023, *A&A*, **677**, L13

Alberton D., et al., 2023, *A&A*, **669**, A93

Alessandrini S., Mattia M., Ningjing J., Luca B., Luca D., Cristina P., 2021, *Molecular Physics*, **119**, e1955988

Aragones J. L., MacDowell L. G., Vega C., 2011, *Journal of Physical Chemistry A*, **115**, 5745

Barnum T. J., et al., 2022, *Journal of Physical Chemistry A*, **126**, 2716

Barone V., 2005, *J. Chem. Phys.*, **122**, 014108

Barone V., 2023a, *The Journal of Physical Chemistry Letters*, **14**, 5883

Barone V., 2023b, *The Journal of Chemical Physics*, **159**, 081102

Barone V., Cimino P., 2008, *Chemical Physics Letters*, **454**, 139

Barone V., Lazzari F., 2023, *The Journal of Physical Chemistry A*, **127**, 10517

Barone V., Bloino J., Guido C. A., Lipparini F., 2010, *Chemical Physics Letters*, **496**, 157

Barone V., Biczysko M., Bloino J., 2014, *Physical Chemistry Chemical Physics (Incorporating Faraday Transactions)*, **16**, 1759

Barone V., Di Grande S., Lazzari F., Mendolicchio M., 2023, *The Journal of Physical Chemistry A*, **127**, 6771

Becke A. D., 1993, *J. Chem. Phys.*, **98**, 5648

Belloche A., Garrod R. T., Müller H. S. P., Menten K. M., 2014, *Science*, **345**, 1584

Bloino J., Barone V., 2012, *J. Chem. Phys.*, **136**, 124108

Boggs J. E., Kim M. G., 1985, *Journal of Molecular Structure: THEOCHEM*, **119**, 271

Bouwman J., Mattioda A. L., Linnartz H., Allamandola L. J., 2011, *A&A*, **525**, A93

Bregman J. D., Hayward T. L., Sloan G. C., 2000, *ApJ*, **544**, L75

Burkhardt A. M., et al., 2021, *apjl*, **913**, L18

Cancès E., Mennucci B., Tomasi J., 1997, *J. Chem. Phys.*, **107**, 3032

Capone L. A., Prasad S. S., Huntress W. T., Whitten R. C., Dubach J., Santhanam K., 1981, *Nature*, **293**, 45

Cernicharo J., Agúndez M., Cabezas C., Tercero B., Marcelino N., Pardo J. R., de Vicente P., 2021a, *A&A*, **649**, L15

Cernicharo J., Agúndez M., Kaiser R. I., Cabezas C., Tercero B., Marcelino N., Pardo J. R., de Vicente P., 2021b, *A&A*, **652**, L9

Chabot M., Béroff K., Dartois E., Pino T., Godard M., 2020, *ApJ*, **888**, 17

Chen T., 2018, *ApJS*, **238**, 18

Chiar J. E., de Barros A. L. F., Mattioda A. L., Ricca A., 2021, *ApJ*, **908**, 239

Cuppen H. M., Walsh C., Lamberts T., Semenov D., Garrod R. T., Penteado E. M., Ioppolo S., 2017, *Space Sci. Rev.*, **212**, 1

Dartois E., d'Hendecourt L., 2001, *A&A*, **365**, 144

Dartois E., d'Hendecourt L., Thi W., Pontoppidan K. M., van Dishoeck E. F., 2002, *A&A*, **394**, 1057

Das A., Acharyya K., Chakrabarti S. K., 2010, *Monthly Notices of the Royal Astronomical Society*, **409**, 789

Das A., Sil M., Gorai P., Chakrabarti S. K., Loison J. C., 2018a, *ApJS*, **237**, 9

Das A., Sil M., Gorai P., Chakrabarti S. K., Loison J. C., 2018b, *The Astrophysical Journal Supplement Series*, **237**, 9

Das A., Sil M., Ghosh R., Gorai P., Adak S., Samanta S., Chakrabarti S. K., 2021, *Frontiers in Astronomy and Space Sciences*, **8**, 78

Doddipatla S., et al., 2021, *Science Advances*, **7**, eabd4044

Duflot D., Toubin C., Monnerville M., 2021, *Frontiers in Astronomy and Space Sciences*, **8**

Dunning Thom H. J., 1989, *J. Chem. Phys.*, **90**, 1007

Esposito V. J., Ferrari P., Buma W. J., Fortenberry R. C., Boersma C., Candian A., Tielens A. G. G. M., 2024, *J. Chem. Phys.*, **160**, 114312

Ferrero S., Zamirri L., Ceccarelli C., Witzel A., Rimola A., Ugliengo P., 2020, *The Astrophysical Journal*, **904**, 11

Flint A. R., Fortenberry R. C., 2022, *ApJ*, **938**, 15

Folsome C. E., Lawless J., Romiez M., Ponnamperuma C., 1971, *Nature*, **232**, 108

Folsome C. E., Lawless J. G., Romiez M., Ponnamperuma C., 1973, *Geochimica Cosmochimica Acta*, **37**, 455

Franke P. R., Stanton J. F., Doubler G. E., 2021, *Journal of Physical Chemistry A*, **125**, 1301

Frisch M. J., et al., 2016, Gaussian~16 Revision C.01

Gardner F. F., Winnewisser G., 1975, *ApJ*, **195**, L127

Gardner J. P., et al., 2006, *Space Sci. Rev.*, **123**, 485

Gorai P., Das A., Sivaraman B., Etim E. E., Chakrabarti S. K., 2017, *The Astrophysical Journal*, **836**, 70

Gordy W., 1953, *Microwave Spectroscopy. Structure of matter series*, Wiley, <https://books.google.co.in/books?id=k98yAAAAMAAJ>

Grimme S., Ehrlich S., Goerigk L., 2011, *Journal of computational chemistry*, **32**, 1456

Hayatsu R., 1964, *Science*, **146**, 1291

Hayatsu R., Studier M. H., Moore L. P., Anders E., 1975, *Geochimica Cosmochimica Acta*, **39**, 471

He J., Acharyya K., Vidali G., 2016, *The Astrophysical Journal*, **825**, 89

Hollis J. M., Jewell P. R., Lovas F. J., 1995, *ApJ*, **438**, 259

Hudgins D. M., Bauschlicher Charles W. J., Allamandola L. J., 2005, *ApJ*, **632**, 316

Keane J. V., Tielens A. G. G. M., Boogert A. C. A., Schutte W. A., Whittet D. C. B., 2001, *A&A*, **376**, 254

Kisiel Z., Desyatnyk O., Pszczółkowski L., Charnley S., Ehrenfreund P., 2003, *Journal of Molecular Spectroscopy*, **217**, 115

Komiya M., Shimoyama A., Harada K., 1993, *Geochimica Cosmochimica Acta*, **57**, 907

Kutner M. L., Machnik D. E., Tucker K. D., Dickman R. L., 1980, *ApJ*, **242**, 541

Lee C., Yang W., Parr R. G., 1988, *Phys. Rev. B*, **37**, 785

Lemmens A. K., Rijs A. M., Buma W. J., 2021, *ApJ*, **923**, 238

Lignell A., Osadchuk I., Räsänen M., Lundell J., 2021, *ApJ*, **917**, 68

Lockman F. J., 1996, in *American Astronomical Society Meeting Abstracts #188*. p. 46.02

Mackie C. J., et al., 2015, *J. Chem. Phys.*, **143**, 224314

Mackie C. J., et al., 2016, *J. Chem. Phys.*, **145**, 084313

Mackie C. J., et al., 2018, *Physical Chemistry Chemical Physics (Incorporating Faraday Transactions)*, **20**, 1189

Martin J. M. L., Lee T. J., Taylor P. R., François J.-P., 1995, *J. Chem. Phys.*, **103**, 2589

Martinez Oscar J., Lattanzi V., Thorwirth S., McCarthy M. C., 2013, *The Journal of Chemical Physics*, **138**, 094316

Martínez-Bachs B., Rimola A., 2023, *International Journal of Molecular Sciences*, **24**

Maté B., Tararro I., Timón V., Cernicharo J., Herrero V. J., 2023, *MNRAS*, **523**, 5887

Matthews H. E., Sears T. J., 1983, *ApJ*, **267**, L53

Matthews D. A., et al., 2020, *J. Chem. Phys.*, **152**, 214108

McCarthy M. C., McGuire B. A., 2021, *Journal of Physical Chemistry A*, **125**, 3231

McCarthy M. C., et al., 2021a, *Nature Astronomy*, **5**, 176

McCarthy M. C., et al., 2021b, *Nature Astronomy*, **5**, 176

McGuire B. A., 2022, *The Astrophysical Journal Supplement Series*, **259**, 30

McGuire B. A., Burkhardt A. M., Kalenskii S., Shingledecker C. N., Remijan A. J., Herbst E., McCarthy M. C., 2018, *Science*, **359**, 202

McGuire B. A., et al., 2021, *Science*, **371**, 1265

McNaughton D., Jahn M. K., Travers M. J., Wachsmuth D., Godfrey P. D., Grabow J.-U., 2018, *Monthly Notices of the Royal Astronomical Society*, **476**, 5268

Mikscha A. M., Riffelt A., Oliveira R., Kästner J., Molpeceres G., 2021, *MNRAS*, **505**, 3157

Molster F. J., et al., 2001, *A&A*, **372**, 165

Mondal S. K., et al., 2021, *ApJ*, **922**, 194

Myers P. C., Thaddeus P., Linke R. A., 1980, *ApJ*, **241**, 155

Pagani L., Favre C., Goldsmith P. F., Bergin E. A., Snell R., Melnick G., 2017, *aap*, **604**, A32

Peeters E., Allamandola L. J., Hudgins D. M., Hony S., Tielens A. G. G. M., 2004, in *Witt A. N., Clayton G. C., Draine B. T., eds, Astronomical Society of the Pacific Conference Series Vol. 309, Astrophysics of Dust*. p. 141 ([arXiv:astro-ph/0312184](https://arxiv.org/abs/astro-ph/0312184)), doi:10.48550/arXiv.astro-ph/0312184

Peng C., Bernhard Schlegel H., 1993, *Israel Journal of Chemistry*, **33**, 449

Pickett H. M., 1991, *Journal of Molecular Spectroscopy*, **148**, 371

Pickett H. M., Poynter R. L., Cohen E. A., Delitsky M. L., Pearson J. C., Müller H. S. P., 1998, *J. Quant. Spectrosc. Radiative Transfer*, **60**, 883

Polehampton E. T., Menten K. M., Brünken S., Winnewisser G., Baluteau J. P., 2005, *A&A*, **431**, 203

Puzzarini C., Stanton J. F., 2023, *Physical Chemistry Chemical Physics (Incorporating Faraday Transactions)*, **25**, 1421

Puzzarini C., Stanton J. F., Gauss J., 2010, *International Reviews in Physical Chemistry*, **29**, 273

Puzzarini C., Alessandrini S., Bizzocchi L., Melosso M., Rivilla V. M., 2023a, *Frontiers in Astronomy and Space Sciences*, **10**, 1211784

Puzzarini C., Linguerri R., Hochlaf M., 2023b, *The Journal of Physical Chemistry A*, **127**, 9502

Puzzarini C., Ye H., Alessandrini S., 2024, *Journal of Computational Chemistry*, **45**, 777

Redondo P., Sanz-Novo M., Barrientos C., 2023, *Monthly Notices of the Royal Astronomical Society*, **527**, 8659

Ricca A., Boersma C., Peeters E., 2021, *ApJ*, **923**, 202

Schilke P., Groesbeck T. D., Blake G. A., Phillips T. G. 1997, *ApJS*, **108**, 301

Sellgren K., Brooke T. Y., Smith R. G., Geballe T. R., 1995, *ApJ*, **449**, L69

Sil M., Gorai P., Das A., Sahu D., Chakrabarti S. K., 2017, *European Physical Journal D*, **71**, 340

Sita M. L., et al., 2022, *apjl*, **938**, L12

Tielens A. G. G. M., 2008, *ARA&A*, **46**, 289

Tomasi J., Mennucci B., Cammi R., 2005, *Chemical Reviews*, **105**, 2999

Tonolo F., Lupi J., Puzzarini C., Barone V., 2020, *ApJ*, **900**, 85

Vats A., Pathak A., 2022, *Monthly Notices of the Royal Astronomical Society*, **517**, 5780

Vats A., Pathak A., Onaka T., Buragohain M., Sakon I., Endo I., 2022, *pasj*, **74**, 161

Vats A., Srivastav S., Pandey A., Pathak A., 2023, *Physical Chemistry Chemical Physics (Incorporating Faraday Transactions)*, **25**, 19066

Vávra K., Luková K., Kania P., Koucký J., Urban Š., 2019, *Journal of Molecular Spectroscopy*, **363**, 111175

Wakelam V., Loison J.-C., Mereau R., Ruaud M., 2017, *Molecular Astrophysics*, **6**, 22

Western C. M., 2017, *jqsrt*, **186**, 221

Woon D. E., 2002, *ApJ*, **571**, L177

Wootten A., Thompson A. R., 2009, *IEEE Proceedings*, **97**, 1463

Yang Q., Mendolicchio M., Barone V., Bloino J., 2021, *Frontiers in Astronomy and Space Sciences*, **8**, 77

van Dishoeck E. F., et al., 2021, *A&A*, **648**, A24

van der Velden W., Schwartz A. W., 1977, *Geochimica Cosmochimica Acta*, **41**, 961

This paper has been typeset from a $\text{\TeX}/\text{\LaTeX}$ file prepared by the author.